Available online at www.sciencedirect.com

ScienceDirect

journal homepage: www.elsevier.com/locate/he

Tafel equation based model for the performance of a microbial fuel cell

G. Hernández-Flores [a], H.M. Poggi-Varaldo [a,*], O. Solorza-Feria [b], M.T. Ponce Noyola [c], T. Romero-Castañón [d], N. Rinderknecht-Seijas [e]

[a] Environmental Biotechnology and Renewable Energies R&D Group, Dept. of Biotechnology and Bioengineering, Centro de Investigación y de Estudios Avanzados del Instituto Politécnico Nacional, Av. Instituto Politécnico Nacional 2508, Col. San Pedro Zacatenco, Delegación Gustavo A. Madero, México D.F., C. P. 07360, Apartado Postal 14-740, 07000 México D.F., Mexico

[b] Dept. of Chemistry, Av. Instituto Politécnico Nacional 2508, Col. San Pedro Zacatenco, Delegación Gustavo A. Madero, México D.F., C. P. 07360 Apartado Postal 14-740, 07000 México D.F., Mexico

[c] Dept. Biotechnology and Bioengineering, Av. Instituto Politécnico Nacional 2508, Col. San Pedro Zacatenco, Delegación Gustavo A. Madero, México D.F., C. P. 07360 Apartado Postal 14-740, 07000 México D.F., Mexico

[d] Electric Research Institute, Reforma 113, Col. Palmira, C. P. 62490 Cuernavaca, Morelos, Mexico

[e] ESIQIE del IPN, Division of Basic Sciences, Escuela Superior de Ingeniería Química e Industrias Extractivas, ESIQIE, Edificio N° 7, Unidad Profesional Adolfo López Mateos. Colonia Lindavista, Delegación Gustavo A. Madero, México D.F., C. P. 07738, Mexico

ARTICLE INFO

Article history:
Received 9 January 2015
Received in revised form
9 May 2015
Accepted 23 June 2015
Available online 5 August 2015

Keywords:
Mathematical model
Volumetric power
Microbial fuel cells

ABSTRACT

The aim of this work was to establish a mathematical model based on Tafel equation to quantitatively relate the maximum volumetric power ($P_{V,max}$) as well as the internal resistance (R_{int}) in a microbial fuel cell (*MFC*) with the specific surface area of the graphite anodes (A'_s), and either their conductance *C* or electrolytic conductivity σ of the material. The anodic chambers of the cells were packed with different anodic materials (graphite rods (*GR*), triangles of graphite (*GT*) and graphite flakes (*GF*), in order of increasing A'_s). The R_{int} decreased and the $P_{V,max}$ increased for cells equipped with *GR*, *GT* and *GF* anodes. There was a correspondence of either the decrease of R_{int} or the increase of $P_{V,max}$ with the increase of the log of A'_s of the graphite anodic materials.

The fitting of the models was characterized in terms of determination coefficient R^2, the *p* value, and the Ranking. The best fitting model for $P_{V,max}$ was $P_{V,max} = a'_0 + a'_1 \times \log A'_s$; with $R^2 = 0.8872$, $p = 0.005$, and Ranking = 100%. The inclusion of *C* as second fitting variable slightly improved the R^2; however, the term with *C* did not have a theoretical origin. For R_{int} the best fitting model was $R_{int} = b'_0 + b'_1 \times \log A'_s$. The model of $P_{V,max}$ was validated with independent results from literature with satisfactory fitting results ($R^2 = 0.8704$; $p = 0.0022$; Ranking = 100%).

* *Corresponding author*. CINVESTAV del IPN, Environmental Biotechnology and Renewable Energy Group, Dept. Biotechnology and Bioengineering, Apartado Postal 14-740, 07000 México D.F., Mexico. Tel.: +52 (55) 5747 3800x4321, +52 (55) 5747 3800x4324.
E-mail address: r4cepe@yahoo.com (H.M. Poggi-Varaldo).

http://dx.doi.org/10.1016/j.ijhydene.2015.06.119

Introduction

The imminent fossil fuels depletion and their adverse effects on the environment have renewed the interest in bioenergies as well as other renewable energy sources [1,2]. In processes such as biohydrogen production from fermentation of organic waste, the complete conversion of waste to energy is not possible [3]. Dark fermentation of organic substrates effects a partial degradation of the organic matter, and typically a large amount of organic metabolites remain in the spent liquors that can be used as substrate in microbial fuel cells (*MFCs*) [4–6].

In this regard, *MFCs* constitute a promising technology for sustainable production of alternative energy and treatment of wastes such as the spent liquors of dark fermentation.

An *MFC* is an electro-biochemical reactor capable of converting organic matter into electricity. In the anodic chamber the microorganisms anaerobically oxidize the organic matter and release electrons and protons. The electrons are transported to the anode that acts as an intermediate, external electron acceptor. Afterwards the electrons collected in the anode flow through an external circuit where there is a resistor or another device. On the other hand, protons travel to the cathode in the liquid phase of the cell and are transported by a special type of membrane (proton exchange membrane) to the cathode. Electrons finally react at the cathode with protons and molecular oxygen, producing water and electricity [5–9].

There are some factors that affect the electric energy production in an *MFC*, such as the nature of the biocatalysts, the type and materials of electrodes, electrode catalysts, cell configuration, and architecture, among others [10–13]. The *MFC* performance is usually restricted by ohmic overpotential, also known as internal resistance (R_{int}). This translates into a loss of voltage that is required to drive the electron and proton transport processes. The ohmic losses in an *MFC* include both the resistance to the flow of electrons through the electrodes and interconnections and the resistance to the flow of ions through the membrane and the anodic and cathodic electrolytes (only anodic electrolyte in a single chamber *MFC*) [14]. This results in ohmic losses whose reduction or mitigation is crucial for improving the characteristics and performance of the *MFC* [15]. Furthermore, another significant role of R_{int} is related to the eventual operation of the *MFC*, since Jacobi's Theorem demonstrated that the maximum power output of an electromotive force is achieved when it is connected to an external resistance (R_{ext}) equal to its R_{int} [14–20].

The R_{int} of a *MFC* depends on some factors such as the surface area of electrodes, distance between electrodes, anodic material conductivity, the presence or absence membrane, the type of electrolyte(s), *inter alia* [14,21,22]. Indeed, the anodic material plays an important role on R_{int}. A good anodic material should have the following properties: high electrical conductivity, strong biocompatibility, chemical stability and anti-corrosion, large surface area and appropriate mechanical strength and toughness [13,14].

In order to reduce the R_{int} of the cell some materials and designs have been evaluated, such as new anodic materials, replacement of the salt bridge by membranes, choosing membranes with high protonic conductivity or building membrane-less *MFC*, increasing solution conductivity and reducing the pH, reducing electrode spacing, among others [5,6,23–29].

Regarding the effect of anodic materials, there has been much research on the use of graphite anodes in *MFC* [11–14,28–35]. However, less has been published on the effect of the specific surface area of graphite anodes on *MFC* characteristics and performance in terms of the volumetric power (P_V). On the other hand, to the best of our knowledge there is little information on modelling the effect of the anodic specific surface area on performance of *MFC* [36–40]. The discussion of former models of *MFC* that took into account the effect of the area or specific surface area of the electrode (anode) includes the critical review of relevant works [36–40]. It can be consulted in the Supplementary Material, Appendix A.

In general, the goals of modelling are quite varied, taking into account the contributions of modelling in Process Engineering, Environmental Science & Engineering, and Physics, Chemistry, and Biological Sciences [41–49]. In our case, the goal of our model was to predict the influence of the specific area of the anodic material on variables related to the electrochemical performance of a *MFC*. The derivation of the model was based on electrochemical principles, whereas the calibration of the parameters was conducted with our own set of experimental results, and subsequent validations were conducted with independent sets of experimental values. Finally, adequacy of model fitting was evaluated by statistical analysis.

Thus, the objective of this work was to establish a mathematical model based on Tafel equation to quantitatively relate the maximum volumetric power ($P_{V,max}$) as well as the R_{int} in a *MFC*, with the specific surface area (A'_s) of the graphite anodes and either their conductance *C* or electrolytic conductivity σ of the material.

Materials and methods

Model development

We describe a full version of the derivation of our model. A typical form of Tafel equation that relates the overpotential with the current density is given by Castellan [50].

$$\Delta V = a + b \times \ln(i) \tag{1}$$

where ΔV is the overpotential, V; b is the "Tafel slope", V; i is the current density, A/m^2.

It can be shown that

$$a = -b \times \ln(i_0) \tag{2}$$

where i_0 is the "exchange current density", A/m^2

Substituting Eq. (2) into Eq. (1), and taking logarithms in base 10 instead of base e, leads to

$$\Delta V = k \log\left(\frac{i}{i_0}\right) \tag{3}$$

where

$$k = b \times 2.303 \tag{4}$$

The actual potential delivered by the MFC can be expressed as the reversible potential minus the overvoltage, as in Eq. (5) [15,20].

$$E = E_{rev} - \Delta V = E_{rev} - k \log\left(\frac{i}{i_0}\right) \tag{5}$$

where E is the actual cell voltage; E_{rev} is the reversible potential (thermodynamic potential [41]), in V; ΔV is the overpotential, in V.

Substituting Eq. (3) into Eq. (5) we obtain the following

$$E = E_{rev} - k \log\left(\frac{i}{i_0}\right) \tag{6}$$

In turn, the power P delivered by the cell is given below [5]:

$$P = \frac{E^2}{R_{ext}} \tag{7}$$

where R_{ext} is the external resistance connected to the cell circuit, in Ω

Substituting Eq. (6) into (7) we obtain the following

$$P = \frac{\left(E_{rev} - k \log\left(\frac{i}{i_0}\right)\right)^2}{R_{ext}} \tag{8}$$

Doing the algebra, taking into account that $\Delta V < E_{rev}$, and that $i = I/A_{el}$, plus some simplifications based on order of magnitude of selected terms, leads to

$$P = \frac{E_{rev}^2 - 2k\log\left(\frac{i}{i_0}\right) + k^2\left(\log\frac{i}{i_0}\right)^2}{R_{ext}} \tag{9}$$

$$P = \frac{E_{rev}^2 - 2k(\log i - \log i_0) + k^2\left[(\log i)^2 - 2\log i{*}\log i_0 + (\log i_0)^2\right]}{R_{ext}} \tag{10}$$

Since $\Delta V < E_{rev}$, we can neglect the term $(\log i_0)^2$ in Eq. (10), leading to

$$P \cong \frac{E_{rev}^2 + 2k\log i_0 - 2k\log i}{R_{ext}} \tag{11}$$

By definition, the current intensity can be expressed as [17,50].

$$i = \frac{I}{A_{el}} \tag{12}$$

where

I is the current intensity in Amperes

A_{el} is the electrode surface area in m^2

Substituting Eq. (12) into Eq. (11) leads to

$$P \cong \frac{E_{rev}^2 + 2k\log i_0 - 2k\log\left(\frac{I}{A_{el}}\right)}{R_{ext}} \tag{13}$$

and

$$P \cong \frac{E_{rev}^2 + 2k\log i_0 - 2k\log I + 2k\log A_{el}}{R_{ext}} \tag{14}$$

$$P \cong \frac{(E_{rev}^2 + 2k\log i_0 - 2k\log I) + 2k\log A_{el}}{R_{ext}} \tag{15}$$

We recall that the A_s' can be determined dividing the electrode surface area A_{el} by the cell volume V_{cell} (the anodic chamber volume in unicameral MFC),

$$A_s' = \frac{A_{el}}{V_{cell}} \tag{16}$$

$$A_{el} = V_{cell}\, A_s' \tag{17}$$

On the other hand, the P_V of a MFC is given by the Eq. (18) below [28].

$$P_V = \frac{P}{V_{cell}} \tag{18}$$

Substituting Eq. (15) in the Eq. (18)

$$P_V \cong \frac{(E_{rev}^2 + 2k\log i_0 - 2k\log I)}{R_{ext} V_{cell}} + \left(\frac{2k}{R_{ext} V_{cell}}\right)\log A_{el} \tag{19}$$

Now, we substitute Eq. (17) in Eq. (19)

$$P_V \cong \frac{(E_{rev}^2 + 2k\log i_0 - 2k\log I)}{R_{ext} V_{cell}} + \left(\frac{2k}{R_{ext} V_{cell}}\right)\log(V_{cell} A_s') \tag{20}$$

Regrouping terms leads to

$$P_V \cong \frac{(E_{rev}^2 + 2k\log i_0 - 2k\log I)}{R_{ext} V_{cell}} + \frac{2k\log V_{cell}}{R_{ext} V_{cell}} + \frac{2k}{R_{ext} V_{cell}}\log A_s' \tag{21}$$

$$P_V \cong \frac{(E_{rev}^2 + 2k\log i_0 - 2k\log I + 2k\log V_{cell})}{R_{ext} V_{cell}} + \frac{2k}{R_{ext} V_{cell}}\log A_s' \tag{22}$$

The first term of the left hand member of Eq. (22) is nearly a constant and it will denoted as a_o, whereas the parameters in the logarithmic term will be denoted as the coefficient a_1. Please note that the E_{rev} in the numerator of a_o is a constant calculated from the standard potentials of the cathodic electron acceptor (typically O_2, half reactions ½ O_2/H_2O) the organic matter half reactor (typically acetate, at least as an example, CO_2/acetate) [51].

Also, the term $2k \times \log V_{cell}$ in the numerator is a constant for a given MFC. Similarly, the term $R_{ext} \times V_{cell}$ in the denominator is a constant since the value of the R_{ext} is set (in particular for the maximum power, the R_{ext} is set equal to R_{int}, as a consequence of Jacobi's theorem for electromotive cells [5,17]). The compounded term $2k \times \log(i_o) - 2k \times \log(I)$ typically cancels out. For instance, for an i_o in the order of 10^{-3} A/m^2 and current intensities I of 10^{-3} A, the corresponding logarithms are in the order of −3 and +3, respectively. Thus, overall, the left term of the right member of Eq. (22) is nearly a constant

$$a_0 = \frac{(E_{rev}^2 + 2k\log i_0 - 2k\log I + 2k\log V_{cell})}{R_{ext} V_{cell}} \tag{23}$$

$$a_1 = \frac{2k}{R_{ext} V_{cell}} \tag{24}$$

Since the Eq. (22) is general, it is also valid in the maximum point of the plot *E-I* of *MFC* characterization, i.e., $P_{V,max}$. Incidentally, at this point, the R_{ext} is equal to R_{int} by Jacobi's theorem [5,17].

So,

$$P_{V,\ max} \cong a_0 + a_1 \log A_s' \tag{25}$$

Now, to estimate the R_{int}, we know that $P_{V,max}$ occurs when the R_{ext} connected to the circuit of an electromotive force is equal to the value of the R_{int}. This is a result of Jacobi's theorem of electromotive forces [17,20,28].

$$R_{int} = R_{ext} \tag{26}$$

By definition of power *P* in direct current circuits and Jacobi's theorem, then

$$P = \frac{(E_{MFC,max})^2}{R_{int}} \tag{27}$$

where

$E_{MFC,max}$ is the cell potential at which the maximum volumetric power is registered. Introducing the volume V_{cell} for converting the power into volumetric power, and solving Eq. (27) for R_{int} leads to

$$R_{int} = \frac{(E_{MFC,max})^2}{V_{cell} \times P_{V,max}} \tag{28}$$

V_{cell} is the cell volume or the anodic chamber volume in a unicameral *MFC*.

Substituting Eq. (25) into Eq. (28) and rearranging

$$R_{int} = \frac{(E_{MFC,max})^2}{V_{cell}} \frac{1}{a_0 + a_1 \log A_s'} \tag{29}$$

$$R_{int} = \frac{(E_{MFC,max})^2}{V_{cell} a_0 \left(1 + \frac{a_1}{a_0} \log A_s'\right)} \tag{30}$$

When a given amount β is $\beta < 1$, the following approximation can be used [52].

$$\frac{1}{1+\beta} \cong 1 - \beta \tag{31}$$

This approximation, although simple, is very good (See Table and Figure with relative errors of Eq. (31) in Supplementary Material, Appendix B). Indeed, it can be shown that when $\beta \leq 0.30$, the error of this formula does not exceed 9%, and when $\beta \leq 0.10$, the error of this formula does not exceed 1% [52].

Using Eq. (31) in Eq. (30) leads to the following approximate result

$$R_{int} \cong \frac{(E_{MFC,max})^2}{V_{cell} a_0} \left(1 - \frac{a_1}{a_0}\right) \log A_s' \tag{32}$$

Rearranging Eq. (32)

$$R_{int} \cong \left(\frac{(E_{MFC,max})^2}{V_{cell} a_0}\right) - \frac{(E_{MFC,max})^2 a_1}{V a_0^2} \log A_s' \tag{33}$$

Now, we conveniently rename the constant coefficients of Eq. (33) as follows

$$b_0 = \frac{(E_{MFC,max})^2}{V_{cell} a_0} \tag{34}$$

$$b_1 = -\frac{(E_{MFC,max})^2 a_1}{V_{cell} a_0^2} \tag{35}$$

Finally, the equation for R_{int} is in the form

$$R_{int} \cong b_0 + b_1 \log A_s' \tag{36}$$

Experimental design

The experiment consisted of the characterization of the *MFC* fitted with the following anodic materials: graphite rods (*GR*), triangles of graphite (*GT*) and graphite flakes (*GF*) in an *MFC* loaded with a sulphate-reducing inoculum (*SR-In*), with two replicates. The main response variables were the $P_{V,max}$ and the R_{int} of the *MFCs*. The experiments were carried out in a single compartment, air-cathode *MFC*. The cells were operated at ambient temperature.

Microbial fuel cell

The *MFC* consisted of a horizontal cylinder built in Plexiglas 80 mm long and 57 mm internal diameter. The anodic chamber was packed with the different anodic materials, i.e., *GR*, *GT* and *GF* with corresponding surface areas of 8.89×10^{-4}, 0.06 and 0.28 m^2 (Table 1, See elementary analyses of graphites in Supplementary Material, Appendix C). The *GR* was obtained from Lumen S. A. de C. V.

The *GTs* were fabricated by conveniently slicing graphite bars of 38 mm diameter in disks of 5 mm thickness. Each disk, in turn, was cut in 8 similar parts. The graphite bar was obtained from Brunssen de Occidente S.A. de C.V.

For *GF*, we screened a large sample of material and collected the fraction between meshes 10 and 6 (diameters 2 mm and 3.55 mm, respectively). We took and weighed five 20 g subsamples of this fraction; the mass values were recorded. Afterwards, the number of particles in each subsample were determined and registered. An average number of particles was estimated. With this number, we estimated the average weight of particle of each material. By using the equations shown below, it was possible to calculate the surface area of the mass of material loaded into the *MFC*. The shape factor of the material (also called sphericity factor in some textbooks) was taken into account as described in Perry [53]. For instance, we chose 0.43 for *GF*.

On the other hand, the net volume of the only chamber in our *MFCs* was calculated as the geometric volume of the chamber minus the physical volume of the anodic material.

With the surface area of the anodic material and the net volume, the A_s' was finally calculated with Eq. (37) below (the complete derivation of Eq. (37) is included in the Supplementary Material, Appendix D).

$$A_s' = \frac{\frac{M}{\varnothing_s}\left(\frac{6^2 m_p^2 \pi^3}{m_p^3 \pi^2 \rho^2}\right)^{1/3}}{V} = \frac{\frac{M}{\varnothing_s}\left(\frac{36\pi}{m_p \rho^2}\right)^{1/3}}{\left(V_{cell} - \frac{M}{\rho}\right)} \tag{37}$$

where

Table 1 – Selected physical characteristics of anodic materials.

Anodic material	Working net volume (m^3)	Anodic actual surface (m^2)	A'_s [a] (m^2/m^3)	Conductance (S) [b]
Graphite rod	2.03×10^{-4}	$8.89 \times 10^{-4} \pm 2.5 \times 10^{-5}$	7.3	0.20 ± 0.04
Triangles of graphite	6.64×10^{-5}	0.062 ± 0.001	931	0.61 ± 0.02
Graphite flakes	7.22×10^{-5}	0.28 ± 0.08	1302	0.13 ± 0.04

Selected physical characteristics of anodic materials.
[a] Relationship between the anode surface area to cell volume, also known as specific surface area of the anode.
[b] Electrical conductance of the materials, expressed in Siemens.

$\varnothing_s$ shape factor of the particle (also called sphericity factor), defined as the quotient of the area of a sphere equivalent to the volume of the particle divided by the actual surface of the particle.
m_p average weight of a particle of the given size fraction
M total mass of anodic material loaded into the *MFC*
ρ actual density of the material
V_{cell} geometric volume of the cell chamber

The surface area of the graphite rod was calculated by geometric calculations based on diameter and height of the rod. The net volume of the *MFC* necessary for the denominator in the calculation of A'_s was estimated as described above in the denominator of Eq. (37).

Similarly, the surface area of graphite triangles was estimated by geometric calculations. For each triangular piece to be loaded into the *MFC*, the total area was the sum of the areas of the two triangular faces ((base times height/2) × 2) plus the areas of the rims. The overall surface area was estimated as the sum of the areas of the pieces. The specific surface area was finally calculated by dividing by the net volume of the *MFC*.

The cathode of our *MFC* was a flexible carbon-cloth containing 0.5 mg/cm^2 platinum catalyst (Pt 10 wt%/C-ETEK). On the air side, the cathode was limited by a perforated plate of stainless steel 1 mm thickness. In the liquid side, the cathode was in contact with a proton exchange membrane (Nafion® 117) [6,54].

Sulphate-reducing inocula

The *MFCs* were seeded with a *SR-In* sampled from a sulphate-reducing complete mix reactor. The biomass concentration in the inoculum was ca. 1280 mg VSS/L. The complete mix bioreactor was operated at 37 °C in a constant temperature room. An influent containing sucrose as carbon source was fed at a flow rate of 120 mL/d to the complete mix sulphate-reducing bioreactor. Its composition was (in g/L): sucrose (5.0), acetic acid (1.5), $NaHCO_3$ (3.0), K_2HPO_4 (0.6), Na_2CO_3 (3.0), NH_4Cl (0.6), Na_2SO_4 (11.0).

Leachate

The *MFC* was loaded with 6 mL of a leachate similar to that produced in the hydrogen fermentation of the organic fraction of the municipal solid wastes [55]. The leachate was prepared by mixing simple organic solvents and organic acids (in g/L): acetic, propionic and butyric acids (4 each) as well as acetone and ethanol (4 each) and mineral salts like $NaHCO_3$ and Na_2CO_3 (3 each) and K_2HPO_4 and NH_4Cl (0.6 each) [56].

Determination of internal resistance of the cell

The R_{int} of the cell was determined by duplicate for each anodic material, using the polarization curve method by varying the R_{ext} and recording both the voltage and the current intensity [6,28]. The *MFC* was operated at open circuit potential (*OCP*) for 1 h; afterwards the R_{ext} was varied from 10 Ω to 1 MΩ and viceversa. After this, the cell was set to open circuit conditions for 1 h in order to check the adequacy of the procedure (values of initial and final *OCP* voltages should be close). The voltage was measured and recorded with a Multimeter ESCORT 3146A. The current was calculated by the Ohm's law and the R_{int} was calculated as the slope of the linear section of the curve voltage versus the current intensity [6,14]. The P_V was calculated according to Logan [28] and Vazquez-Larios et al. [6].

The initial chemical oxygen demand (*COD*) and biomass concentration in the cell liquor were *ca.* 1300 mg O_2/L and 1280 VSS/L, respectively. The pH and the electrical conductivity were 7.03 and 1385 μS/cm, respectively.

Analyses

The *COD* and *VSS* of the liquors of sulphate-reducing seed bioreactor and cells were determined according to the Standard Methods [57–59]. In addition, the individual concentrations of volatile organic acids and solvents in the model extract were analysed by gas chromatography in a chromatograph Perkin Elmer Autosystem equipped with a flame ionization detector as described elsewhere [6,60].

Statistical data processing was performed with the tool Analysis of Data of Excel software, Microsoft Office 2010 (Microsoft, Seattle, WA, USA). Excel outputs were checked with Minitab 17 results (Minitab Inc., State College, PA, USA) as a quality control; both softwares gave identical results.

Results and discussion

Characterization of the cell using the anodic materials and sulphate-reducing inocula

Table 1 exhibits some properties of the anodic materials whereas Fig. 1a shows the characterization of the *MFC* fitted with *GR* as anode. The maximum *OCP* was 800 mV in the first hour of the characterization; at the end of the procedure the

OCP was 600 mV. A few factors could have influenced a lower OCP in the backwards procedure of the polarization test, such as substrate consumption, development of substrate gradients with lower concentrations in the proximity of the anode at the end of the polarization test, to name a few. We recall that the content of our MFC was not mixed, and the cell was operated at ambient temperature. From the biocatalyst point of view, it is likely that the planktonic inoculum probably could have settled at the end of the test, given the lack of mixing of the MFC. Moreover, since the polarization test is relatively short compared to the duplication times of anaerobic bacteria present in the anodic chamber, it is not probable that there was enough time to foster the formation of bacterial biofilms on the anodes. The R_{int} was obtained from the slope of graph voltage *vs.* current intensity and gave a value of 795 Ω (Table 2).

With GT as anode, the estimated R_{int} was 410 Ω (50% lower than the R_{int} obtained by the GR) and the $P_{V,max}$ reached 2108 mW/m^3 (Fig. 1b, Table 2).

P_V improved by 60% using the GT (Table 2). It is interesting to note that the ratio between specific surface areas of the corresponding anodes (anodic surface/cell volume) increased by 12,700% from GR to GT (a ratio 931/7.3; Table 1). This could partially explain the lower R_{int}, although neither the power increase nor the R_{int} decrease was in the same proportion ratio as the anodic surface area increase.

Regarding the GF used as anode, the R_{int} and $P_{V,max}$ decreased and increased respectively with respect to GT as anode (Fig. 2, Table 2). The R_{int} was 35% lower than GT and the $P_{V,max}$ reached 3052 mW/m^3, 45% more than GT. It is important to note that in this anode, the relationship anodic surface/cell volume increased 4 times from GT to GF (Table 1).

Table 2 – Results of characterization of the microbial fuel cells.

Parameters	Graphite rod	Triangles of graphite	Graphite flakes
Inoculum	SR-In[a]	SR-In	SR-In
R_{int} (Ω)	795 ± 147	410 ± 22	273 ± 153
$P_{s,max}$ (mW/m^2)[b]	65.4 ± 0.1	54 ± 0.1	86.4 ± 0.7
$P_{V,max}$ (mW/m^3)[c]	1326 ± 72	2108 ± 174	3052 ± 23
P_{max} (mW)	0.17 ± 0.01	0.14 ± 0.01	0.22 ± 0.01
I_{max} (mA)[d]	1.53 ± 0.3	1.92 ± 0.6	3.50 ± 0.6
$E_{MFC,max}$ (mV)[e]	700 ± 1	500 ± 1	402 ± 1
$E_{MFC,OC}$ (mV)[f]	800 ± 120	600 ± 140	575 ± 33

[a] Sulphate-reducing inoculum.
[b] Maximum power density based on surface area of electrode (cathode).
[c] Maximum volumetric power.
[d] Current intensity value at the maximum power.
[e] Potential value at the maximum power.
[f] Open circuit potential.

The larger surface area of GF compared to the other anodic materials would be an advantage since the microorganisms would have a greater anodic surface to colonize and transfer the electrons. Indeed, besides the surface area, the architecture, texture, and roughness of the surface of the support material can play a significant role on the colonization and charge transfer process in MFC [28,61], as well as in the microbial colonization in other microbial processes of pollution control [62,63]. For instance, Kano et al. [61] observed that the micro scale surface topography of anodes strongly affected the performance of MFC. They tested seven types of anode electrode with different micro scale surface topography, and observed that MFC performance depended on the contact areas between the bacteria and anode. In effect, the maximum power was recorded for the cell equipped with the anode containing micro holes 5–7 μm in diameter.

In this regard, our results and interpretation are consistent with findings of other researchers [31–35]. Hays et al. [31] observed that MFC equipped with graphite fibre brush

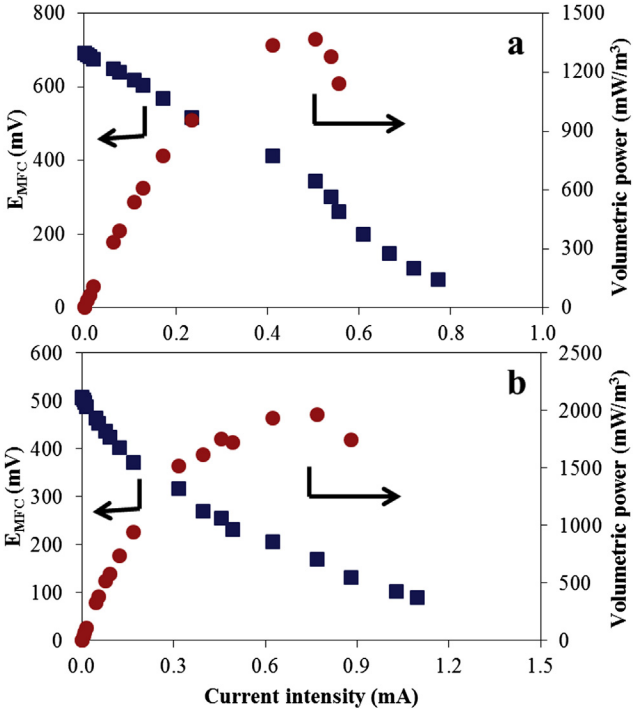

Fig. 1 – Characterization of the microbial fuel cell fitted either with graphite rod and graphite triangles as anode: (a) Polarization curve and volumetric power for graphite rod as anode; (b) Polarization curve and volumetric power with graphite triangles as anode.

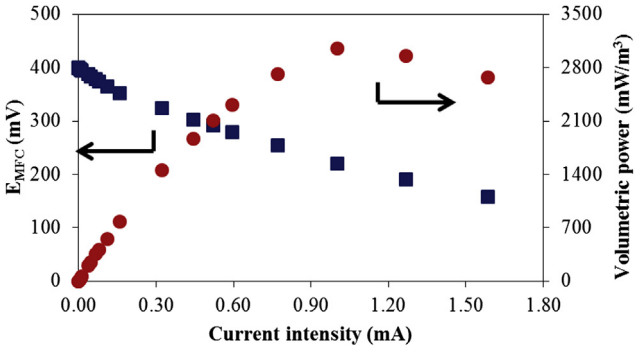

Fig. 2 – Polarization curve and volumetric power with graphite flakes as anode.

electrodes and modified designs (separators with graphite brush electrodes, to make a more compact design) gave satisfactory power and potential outputs. They ascribed this to high surface areas for exoelectrogenic bacteria growth in graphite-brush-equipped *MFCs*. Feng et al. [32] studied the treatment of carbon fibre brush anodes for improving the power output in an air-cathode *MFCs*. They concluded that carbon brush electrodes provided high surface areas for bacterial growth and high power densities in *MFCs*. Larrosa-Guerrero et al. [33] examined the effect of various carbon anodes (graphite, sponge, paper, cloth, felt, fibre, foam and reticulated vitreous carbon (*RVC*)) on *MFC* performance. The influent was brewery wastewater diluted with domestic wastewater. Biofilms were grown at open circuit or under an external load. The average voltage output was 600 mV at closed circuit when connected to an external resistance of 300 kΩ, and 750 mV at open circuit for all materials, except *RVC*. They observed a poor performance of *RVC* compared to the other anodic materials, *i.e.*, power densities as low as 1.3 mW/m^2. The authors concluded that this might be related to lower surface area available and concentration polarization caused by the morphology of the material and the structure of the biofilm.

Liu et al. [34] observed that the achievable maximum current density for mature microbial biofilms in *MFC* treating wastewater depended strongly on the electrode material and size, among other factors. Incidentally, the potential of the active site (−120 mV vs. SHE) was similar for all the electrocatalytically active microbial biofilms in their work, and to that observed for *Geobacter sulfurreducens* in other works. Such improvement in *MFC* performance correlated with the increased surface area and the change of surface functional groups as revealed by X-ray photoelectron spectroscopy analysis. Also, the authors concluded that the anode material type and surface area are considered key factors influencing the energy conversion in *MFCs* because it links microbiology and electrochemistry.

The good characteristics of *MFC* fitted with graphite anodes in our work (*i.e.*, *GR*, *GT* and *GF*) could be explained, at least in part, by the high electric conductivity of graphite (Table 1).

Modelling of the maximum volumetric power and internal resistance of microbial fuel cells equipped with graphite anodes in this work

We made an attempt to quantitatively relate the $P_{V,max}$ and R_{int} in this work to the A'_s of the graphite anodes as well as either the *C* or σ of the material. We have used the six datasets for model fitting, *i.e.*, two replicates for each anodic material (3 × 2). A theoretical development that linked the P_V to the cell potential (and the latter, in turn, was expressed as the reversible potential minus the overpotential described by Tafel equation, see Section 2.1 for model derivation) showed that $P_{V,max}$ and R_{int} could be associated to the log A'_s, Eqs. (31) and (42).

Consequently, we postulated linear models of R_{int} and $P_{v,max}$ in terms of:

- the specific surface area of the electrode A'_s or its logarithm,
- the conductance *C* of the material of the electrode or its logarithm,
- the electrolytic conductivity σ of the material of the electrode or its logarithm

A family of one-variable linear models and two-variable models, without and with interaction between fitted variables were fitted to our experimental data. Table 3 shows detailed statistical information on the fitting of several models tested in our work. The selection of the recommended models was based on these criteria:

(i) Among models with similar goodness of fit, we select the one or those that has/have a theoretical basis over the ones that are only empirical.
(ii) Among models with similar or reasonable fitting goodness, it was decided to choose simplified expressions because, in addition to the attractive simplicity, the model will have higher degrees of freedom.
(iii) We recommend models that exhibit the lowest value of probability of the Fisher statistic *p(F)*; low values are related to higher significance of the ANOVA.
(iv) Models with high values of determination coefficient are good candidates for final selection, provided that other statistical parameters of the model are also satisfactory.
(v) Models with high values of the parameter *Ranking* will be preferred, provided that other statistical and fitting parameters are also satisfactory. In this regard, we have defined a convenient parameter *Ranking* as follows:

$$Ranking = \left(\frac{Number\ of\ significant\ fitting\ coefficients}{Number\ of\ total\ coefficients}\right) \times 100 \quad (38)$$

In this work, a fitting coefficient equation is defined as 'significant' (stands for 'this work') when its confidence interval 95% does not contain the zero (0), although the statistical significance of a coefficient is typically given by the corresponding value *p(T)*. Generally, a low value of *p(T)* indicates a statistically significant coefficient.

Based on the application of these criteria we have chosen five models that adequately fitted our experimental results. Three models for the $P_{V,max}$ (Eq. (39) and (41); models 1, 3, and 5; Table 3) and two models for the R_{int} of the *MFC* (Eqs. (42) and (43); models 2, 16; Table 3).

$$1.\ P_{V,max} \cong a'_0 + a'_1 \log A'_s \quad (39)$$

$$3.\ P_{V,max} \cong a_0 + a_1 \log A'_s + a_2 \times C \quad (40)$$

$$5.\ P_{V,max} \cong a'_0 + a'_1 \times \log A'_s + a'_2 \times \log C \quad (41)$$

$$2.\ R_{int} \cong b'_0 + b'_1 \times \log A'_s \quad (42)$$

$$16.\ R_{int} \cong b_0 + b_1 \times \log A'_s + b_2 \times \sigma + b_{12} \times \left[\left(\log A'_s\right) \times \sigma\right] \quad (43)$$

Among these models, we feel that the most suitable are the No 1 and 2 (Eqs. (39) and (42)) since they show an adequate set of statistical parameters and at the same time are the most

Table 3 – Model fitting of either maximum volumetric power or internal resistance with the specific area of anodes and other variables this work.

Model regression equation	R^2[a]	a'_0 or b'_0[b]	a'_1 or b'_1[c]	a'_2 or b'_2[d]	a'_{12} or b'_{12}[e]	*Ranking*[f] (%)	*p(F)*[g]
1. $P_{V,max} = a_0' + a_1' \times \log A'_s$	0.8872	842.9*	633.2*	NA[h]	NA	100	0.005
2. $R_{int} = b_0' + b_1' \times \log A'_s$	0.8850	933.5*	−211.6*	NA	NA	100	0.005
3. $P_{V,max} = a_0 + a_1 \times \log A'_s + a_2 \times C$	0.9842	1133.66*	660.73*	−1046.79*	NA	100	0.002
4. $R_{int} = b_0 + b_1 \times \log A'_s + b_2 \times C$	0.8865	922.15*	−212.75*	43.69	NA	67	0.038
5. $P_{V,max} = a_0' + a_1' \times \log A'_s + a_2' \times \log C$	0.9810	403.2	629.8*	−738.69*	NA	67	0.003
6. $R_{int} = b_0' + b_1' \times \log A'_s + b_2' \times \log C$	0.8904	968.9*	−211.3*	59.46	NA	67	0.036
7. $P_{V,max} = a_0 + a_1 \times \log A'_s + a_2 \times C + a_{12} \times [(\log A'_s) \times C]$	0.9861	1569.97	493.39	−3387.82	917.61	0	0.021
8. $R_{int} = b_0 + b_1 \times \log A'_s + b_2 \times C + b_{12} \times [(\log A'_s) \times C]$	0.9124	353.21	−4.11	2962.56	−1144.1	0	0.128
9. $P_{V,max} = a_0' + a_1' \times \log A'_s + a_2' \times \log C + a_{12}' \times [(\log A'_s) \times (\log C)]$	0.9833	−402.11	949.48	−1864.23	427.92	0	0.025
10. $R_{int} = b_0' + b_1' \times \log A'_s + b_2' \times \log C + b_{12}' \times [(\log A'_s) \times (\log C)]$	0.9081	1720.77	−509.79	1110.44	−399.57	0	0.135
11. $P_{V,max} = a_0 + a_1 \times \log A'_s + a_2 \times \sigma$	0.9277	−318.23	1026.97*	1.61	NA	33	0.019
12. $R_{int} = b_0 + b_1 \times \log A'_s + b_2 \times \sigma$	0.9052	658.72	−118.45	0.38	NA	0	0.029
13. $P_{V,max} = a_0 + a_1' \times \log A'_s + a_2' \times \log \sigma$	0.9732	−3583.09	1507.69*	1423.86	NA	33	0.004
14. $R_{int} = b_0' + b_1' \times \log A'_s + b_2' \times \log \sigma$	0.8918	517.10	−129.35	133.94	NA	0	0.036
15. $P_{V,max} = a_0 + a_1 \times \log A'_s + a_2 \times \sigma + a_{12} \times [(\log A'_s) \times \sigma]$	0.9401	−382.66	1286.00	10.09	−13.47	0	0.089
16. $R_{int} = b_0 + b_1 \times \log A'_s + b_2 \times \sigma + b_{12} \times [(\log A'_s) \times \sigma]$	0.9923	715.79*	−347.90*	−7.13*	11.93*	100	0.012
17. $P_{V,max} = a_0' + a_1' \times \log A'_s + a_2' \times \log \sigma + a_{12}' \times [(\log A'_s) \times (\log \sigma)]$	0.9732	−3581.61	1514.17	1425.54	−5.78	0	0.040
18. $R_{int} = b_0' + b_1' \times \log A'_s + b_2' \times \log \sigma + b_{12}' \times [(\log A'_s) \times (\log \sigma)]$	0.9595	350.38	−857.95	−54.84	649.40	0	0.060

*The star on the right side of the coefficients values means that their values were statistically significant and that zero did not belong to their 95% confidence intervals.

[a] Determination coefficient.

[b] Independent term of the equation.

[c] Coefficient of the variable log A'_s.

[d] Coefficient of the second variable C, σ, log C or log σ.

[e] Coefficient of the third variable 'crossed product' of the first and second variable.

[f] Ranking = (Number of significant coefficients of the regression/Number of total coefficients)*100; 'significant coefficients' are those whose confidence interval does not include zero (0).

[g] Probability of the Fisher statistics in the ANOVA of the regression.

[h] Not applicable.

simple (one independent variable) and their mathematical forms are based on a theoretical derivation (Tafel equation for overvoltage of the MFC plus ancillary concepts). Standardized residuals of our selected models were higher than −2 and lower than 2, which suggests the absence of outliers [64].

As a worked example on how the selection process proceeds, let us focus the attention on model 17 for $P_{V,max}$ (Table 3). This model was not chosen to represent our data in spite that shows a high R^2, because.

- the model is more complex (3 independent variables, or two independent variables plus their interaction, as one prefers to consider it),
- two terms of the model are not related to basic electrochemical mechanisms of the device (the second and the third terms of the right member), in fact, these two terms could be considered as mere empirical contributions,
- the *p(F)* of the ANOVA of the model is relatively high compared to those of other models
- the *Ranking* is 0%, that is, the confidence intervals of all the fitting coefficients contain zero (0).

To the best of our knowledge there is little information on modelling the effect of the A'_s on performance of MFC [36–40,65] in terms of P_V. For instance, Hsu et al. [36] fitted the current intensity *i* to the anode surface area. This model gave an inverse relationship between the variables.

$$i = \frac{(mE_{anode} + b)}{A_{anode}} \quad R^2 \text{ not reported} \tag{44}$$

where *i* is the current density, E_{anode} is the anodic potential, A_{anode} is the surface area of the anode, m and b are fitting coefficients. Incidentally, Hsu et al. [36] experimentally observed, but did not model, the decrease of the surface power densities P_{An} when the anode surface area was increased. They reported the values of P_{An} but they neither modelled the effect of the anodic surface area (or the A'_s) on that variable nor the P_V of the cell. To some extent, the decrease of P_{An} with increase of anode area should be expected whenever the increase of P_{MFC} is less than proportional to such an area. Furthermore, the model of Hsu et al. [36] was strictly empirical since it was not based upon electrochemical theoretical considerations. The authors did not report statistical parameters of the model, and consequently, it is very difficult to ascertain the fitting goodness of the proposed equation.

Dewan et al. [37] worked with several anodic areas (graphite plates) in a two-chamber MFC. They modelled the P_{An} versus the logarithm of the *total* surface area of the anode. They found a linear, decreasing relationship (Eq. (45), $R^2 = 0.95$). It can be seen that the coefficient of the term ln (surface area) is negative, which was consistent with the experimental results of Hsu et al. [36]. As we commented above, it is debatable to use P_{An} as a variable for comparison of

process intensity. In this regard, P_V is the dependent variable of choice. On the other hand, P_{An} is an adequate variable to assess anode performance. The model fitted by Dewan et al. [37] was strictly empirical since it was not based upon electrochemical theoretical considerations. No statistical parameters of fitting goodness were reported, other than R^2.

$$P_{An} = 0.3371 - 0.0369 \times \ln(surface\ area)\ R^2 = 0.95 \quad (45)$$

Di Lorenzo et al. [38] presented a "Current distribution model" that found a relationship between a variable ν (the so-called 'utilization of the electrode area' in Siemens $^{0.5}$/sec) with a set of independent variables of electrode geometry ('L', thickness of the anode; 'a', specific area of the anode), the slope of the polarization curve 's', and the conductivity of the influent κ.

$$\mathrm{v} = \mathrm{L} \times \left(\frac{a \times \mathrm{s}}{k}\right)^{0.5} \quad (46)$$

They departed from theoretical grounds (Butler-Volmer kinetics in the anode) and several simplifying assumptions. They also defined a new variable efficiency η related to ν by Eq. (47).

$$\eta = \frac{\tanh(\nu)}{\nu} \quad (47)$$

be useful as a starting point in selecting electrode geometries based on basic data of the influent and electrode conductivity.

Interestingly, the use of either i or P_{An} in the above mentioned models is very debatable as a means to express the *MFC* performance when the purpose is to compare the process intensity (unit power delivery) of a given *MFC* with the intensity of other competing processes such as anaerobic digestion, biohydrogen generation, other *MFC* configurations, etc., which could use the same influent as the main experiment.

The purpose of the work by Merkey & Chopp [39] was to examine the competition for space and nutrients of conductive and mediator-using bacteria in a *MFC*, assuming a biofilm populated by both types of species. The model considered 41 parameters and 9 variables. The specific area of the anode was considered to have a fixed value in this work. Unfortunately, they neither considered the specific area of the anode as a variable itself nor evaluated its effect on the output of the model. The emphasis of the model was on microbiological features. Incidentally, the microbiological predictions from simulation runs using their model were not validated.

In another paper, Merkey & Chopp [40] sought to examine the dependence of *MFC* power output on electrode geometry and other operational parameters when electron transfer occurs through a conductive biofilm. Their model considered 21

$$\eta = \frac{\text{observed current density}}{\text{current obtained if the electrode potential was equal to the maximum observed at position L in the electrode}} \quad (48)$$

As a working example of their model, the authors calculated the current density peak i_2 during batch operation of a *MFC* based on a known current density peak i_1, the corresponding values of L (L_1 and L_2), and the corresponding values of η, with an equation (not given by the authors and recreated by us).

$$i_2 = i_1 \times \left(\frac{L_2}{L_1}\right) \times \left(\frac{\eta_2}{\eta_1}\right) \quad (49)$$

They showed that their model could give reasonable results compared to experimental values of current density peaks in a couple of their experimental cases. However, in their work, (i) they did not develop any general fitting of Eq. (46)–(48). Furthermore, they did not report any statistical measure of fitting goodness (no determination coefficients, no ANOVA of the model equations and predictions, etc.); (ii) they did not fit any model with P_V or R_{int} as dependent variable and the A'_s as independent variable, i.e., their model was used just to approximately predict current density peaks but not powers (neither P_V nor P_{An}); and (iii) the physical meaning of the variable ν given by the authors is vague. Furthermore, in spite of considerable workload to develop an expression forν, this variable is only used as a 'transition' one in order to calculate the corresponding value of η.

In the end, Di Lorenzo et al. [38] concluded that, in spite of several recognized simplifying assumptions, the model could parameters and 7 variables. Neither the anodic area nor the specific area of the anode was considered in the parameter set or the variable set of this work. The authors warned that their model intended to elucidate the trends that one would expect to see in a *MFC*, and was not meant to make precise predictions regarding the power output. Furthermore, the predictions based on the simulation runs were not validated.

The fitting of our model to data published by Dewan et al. [37] was also performed. Their goal was to quantify the relationship, if any, between the surface area of the anode of a two-chamber *MFC* and the anodic power density (surface). Graphite plate electrodes of various sizes were used as anodes. The cathode consisted of Mn-based catalysed carbon bonded to a Pt mesh that performed as current-collector device. They found that the power density (surface) P_{An} decreased as the surface area of the anode increased; the relationship was decreasingly linear when the P_{An} was plotted against log of the surface area of the anode. Unfortunately, they neither used the *specific surface area* A'_s of the anode (just the plain surface area) nor performed any study on the relationship between the P_V and A'_s. From data in their 'Materials and Methods' section as well as their results from the 'Results and discussion' section (Fig. 2b in their article), we calculated the $P_{v,max}$ and the A'_s. Afterwards, we applied our most simple model $P_{V,max}$ versus log (A'_s) (Model 1 in Table 3, Eq. (40)). We found that our model adequately fitted their experimental results (Eq. (50) below).

$$P_{V,\ max} \cong 0.0348 + 0.01437 \times \log A'_s \quad (50)$$

with $P_{V,max}$ in mW/cm^3, A'_s in cm^2/cm^3

The statistical parameters were the following:

$R^2 = 0.8704;\ p(F) = 0.0022;\ Ranking = 100\%$
$0.02347 \leq a_o \leq 0.04469$at 95% confidence, $p(T) = 0.00042$
$0.00800 \leq a_1 \leq 0.02075$ at 95% confidence, $p(T) = 0.00216$

The largest standardized residual was 1.43, whereas the smallest was −1.22. Thus, all the residuals fell in the interval (−2.0, 2.0) meaning that no outliers were found [64].

At this point, it is worth comparing our model with the previous models available in the literature. The latter dealt with cell performance and the surface area of the anode but focused on other dependent variables that are not useful indicators of process intensity, such as current intensity [36], peaks of current intensity [38], or P_{An} [36]. This was a first shortcoming, since the use of either i or P_{An} is not the most adequate variable to express the *MFC* performance when the purpose is to compare the process intensity with intensity of other competing processes as we discussed above.

Two of the three previous models presented in the literature did not report statistical parameters that show the goodness of fit. Only one of them [37] reported the determination coefficient R^2, but no information on $p(F)$, confidence intervals of the fitting coefficients, *etc.*, was included. So, the usefulness of such models as well as their fitting goodness is difficult to assess. Only one of the previous models out of the three has been based on electrochemical theoretical grounds [38]. The other two are strictly empirical [36,37].

In contrast, our model focuses on the relationship of the volumetric power and internal resistance versus the specific area of anode, and it is based on electrochemical theory (Tafel equation and ancillary concepts). Moreover, thorough statistical evidence of its goodness-of-fit is provided.

Conclusion

The type and size of anodic material had a significant effect on the R_{int} and $P_{V,max}$ of *MFCs* in our work. Comparing the graphite anodes, the $P_{V,max}$ increased and the R_{int} decreased in three materials (*GR*, *GT* and *GF*) with the increase of the log of the specific surface area of the anode. A theoretical model for the $P_{V,max}$ and R_{int} based on the electrochemical performance of the cell lead to equations that satisfactorily fitted the experimental results.

The mathematical model leads us to predict the behaviour of the performance of the *MFCs*. It is very important in order to scaling these devices. Our model overcomes limitations of previous models published in the open literature that attempted to relate A'_s to electrochemical performance variables of *MFCs*. To the best of our knowledge, it is the first to quantitatively relate the P_V of *MFCs* to the logarithm of the A'_s, departing from theoretical knowledge and leading to a relatively simple model.

Acknowledgements

The authors gratefully acknowledge the input and suggestions of the Editors and Reviewers, which allowed us to significantly improve the manuscript. The authors also wish to thank CINVESTAV-IPN and ICYTDF (now SECITI-GDF), Mexico, for financial support to this research (PICCO-10-28), and CONACYT for the Infrastructure Project 188281. Mr Giovanni Hernández-Flores, Sc D candidate, received a graduate scholarship from CONACYT, Mexico. The excellent technical help of Mr. Rafael Hernández-Vera and technicians of the Environmental of Biotechnology and Renewable Energy R&D Group, CINVESTAV-IPN, is appreciated. The authors acknowledge the technical help of Mr. Álvaro Ángeles Pascual, Research Associate, M. Sc., of the Advanced Laboratory of Electronic Nanoscopy, CINVESTAV-IPN, with XRD analysis of the anodic materials used in our work.

Appendix A. Supplementary data

Supplementary data related to this article can be found at http://dx.doi.org/10.1016/j.ijhydene.2015.07.038.

REFERENCES

[1] Das D, Veziroglu TN. Hydrogen production by biological processes: a survey of literature. Int J Hydrogen Energy 2001;26:13–28.
[2] Cheng-Dar Y, Chung-Ming L, Liou EML. A transition toward a sustainable energy future: feasibility assessment and development strategies of wind power in Taiwan. Energy Policy 2001;29:951–63.
[3] Valdez-Vázquez I, Ríos-Leal E, Esparza-García FJ, Cecchi F, Poggi-Varaldo HM. Semi-continuous solid substrate anaerobic digestors for H_2 production from organic waste: mesophilic versus thermophilic regime. Int J Hydrogen Energy 2005;30:1383–91.
[4] Valdez-Vazquez I, Rios-Leal E, Carmona-Martinez A, Muñoz-Páez K, Poggi-Varaldo HM. Improvement of biohydrogen production from solid wastes by intermittent venting and gas flushing of batch reactors headspace. Environ Sci Technol 2006;40:3409–15.
[5] Poggi-Varaldo HM, Carmona-Martínez A, Vázquez-Larios AL, Solorza-Feria O. Effect of inoculum type on the performance of a microbial fuel cell fed with spent organic extracts from hydrogenogenic fermentation of organic solid wastes. J New Mater Electrochem Syst 2009;12:49–54.
[6] Vazquez-Larios AL, Solorza-Feria O, Vazquez-Huerta G, Esparza-Garcia FJ, Rios-Leal E, Rinderknecht-Seijas N, et al. A new design improves performance of a single chamber microbial fuel cell. J New Mater Electrochem Syst 2010;13:219–26.
[7] Du Z, Li H, Gu T. A state of the art review on microbial fuel cells: a promising technology for wastewater treatment and bioenergy. Biotechnol Adv 2007;25:464–82.
[8] Lefebvre O, Al-Mamun A, Ooi WK, Ng HY, Tang Z, Chua DHC. An insight into cathode options for microbial fuel cells. Water Sci Technol 2008;57:2031–7.
[9] Ouitrakul S, Sriyudthsak M, Charojrochkul S, Kakizono T. Impedance analysis of bio-fuel cell electrodes. Biosens Bioelectron 2007;23:721–7.
[10] Belleville P, Strong PJ, Dare PH, Gapes DJ. Influence of nitrogen limitation on performance of a microbial fuel cell. Water Sci Technol 2011;63:1752–7.
[11] Logan BE, Regan JM. Microbial challenges and harnessing the metabolic activity of bacteria can provide energy for a variety

of applications, once technical and cost obstacles are overcome. Environ Sci Technol 2006:5172–80.
[12] Yang Y, Sun G, Xu M. Microbial fuel cells come of age. J Chem Technol Biotechnol 2010;86:625–32.
[13] Zhou M, Chi M, Luo J, He H, Jin T. An overview of electrode materials in microbial fuel cells. J Power Sources 2011;196:4427–35.
[14] Logan BE, Hamelers B, Rozendal R, Schröder U, Keller J, Freguia S, et al. Microbial fuel cells: methodology and technology. Environ Sci Technol 2006;40:5181–92.
[15] Rismani-Yazdi H, Carver SM, Christy AD, Tuovinen OH. Cathodic limitations in microbial fuel cells: an overview. J Power Sources 2008;180:683–94.
[16] Halliday D, Resnick R, Walker J. Fundamentals of physics. 7th ed. New York: John Wiley & Sons, Inc; 2005. ISBN:978-0-471-21643-8.
[17] Halliday D, Resnick R, Walker J. Fundamentals of physics. 9th ed. New York: John Wiley & Sons, Inc; 2011. ISBN:978-0-471-21643-8.
[18] Jiang D, Li B. Novel electrode materials to enhance the bacterial adhesion and increase the power generation in microbial fuel cells (MFCs). Wat Sci Technol 2009;59(3):557–63.
[19] Logan BE. Simultaneous wastewater treatment and biological electricity generation. Water Sci Technol 2005;52:31–7.
[20] Poggi-Varaldo HM, Vazquez-Larios A, Solorza-Feria O. Microbial fuel cells. In: Rodríguez-Varela FJ, Solorza-Feria O, Hernández-Pacheco E, editors. Fuel cells. Book Livres, Montréal, Canada; 2010. p. 124–61.
[21] Li F, Sharma Y, Lei Y, Li B, Zhou Q. Microbial fuel cells: the effects of configurations, electrolyte solutions, and electrode materials on power generation. Appl Biochem Biotechnol 2011;160:168–81.
[22] Torres CI, Marcus AK, Lee HS, Parameswaran P, Krajmalnik-Brown R, Rittmann BE. A kinetic perspective on extracellular electron transfer by anode-respiring bacteria. Bioresour Technol 2010;102:9335–44.
[23] Rabaey K, Lissens G, Steven DS, Verstraete W. A microbial fuel cell capable of converting glucose to electricity at high rate and efficiency. Biotechnol Lett 2003;25:1531–5.
[24] Liu H, Logan BE. Electricity generation using an air-cathode single chamber microbial fuel cell in the presence and absence of a proton exchange membrane. Environ Sci Technol 2004;38:4040–6.
[25] Min B, Cheng S, Logan BE. Electricity generation using membrane and salt bridge microbial fuel cells. Water Res 2005;39:1675–86.
[26] Liu H, Cheng S, Logan BE. Power generation in fed-batch microbial fuel cells as a function of ionic strength, temperature, and reactor configuration. Environ Sci Technol 2005;39:5488–93.
[27] Cheng S, Liu H, Logan BE. Increased power generation in a continuous flow MFC with advective flow through the porous anode and reduced electrode spacing. Environ Sci Technol 2006;40:2426–32.
[28] Logan BE. Microbial fuel cells. New Jersey, USA: John Wiley-Interscience; 2007.
[29] Jiang D, Li B. Granular activated carbon single-chamber microbial fuel cells (GAC-SCMFCs): a design suitable for large-scale wastewater treatment processes. Biochem Eng J 2009;47:31–7.
[30] Wei J, Xia LP,H. Recent progress in electrodes for microbial fuel cells. Bioresour Technol 2011;102:9335–44.
[31] Hays S, Zhang F, Logan BE. Performance of two different types of anodes in membrane electrode assembly microbial fuel cells for power generation from domestic wastewater. J Power Sources 2011;195:8293–300.
[32] Feng Y, Yang Q, Wang X, Logan BE. Treatment of carbon fiber brush anodes for improving power generation in air–cathode microbial fuel cells. J Power Sources 2010;195:1841–4.
[33] Larrosa-Guerrero A, Scott K, Katuri KP, Godinez C, Head IM, Curtis T. Open circuit versus closed circuit enrichment of anodic biofilms in MFC: effect on performance and anodic communities. Appl Microbiol Biotechnol 2010;87:1699–713.
[34] Liu Y, Harnisch F, Fricke K, Schröder U, Climent V, Feliu JM. The study of electrochemically active microbial biofilms on different carbon- based anode materials in microbial fuel cells. Biosens Bioelectron 2010;25:2167–71.
[35] Jin T, Zhou L, Luo J, Yang J, Zhao Y, Zhou M. Hydrazine hydrate chemical reduction as an effective anode modification method to improve the performance of microbial fuel cells. J Chem Technol Biotechnol 2013;88:2075–81.
[36] Hsu L, Chadwick B, Kagan J, Thacher R, Wotawa-Bergen A, Richter K. Scale up considerations for sediment microbial fuel cells. RSC Adv 2013;3:15947–54.
[37] Dewan A, Beyenal H, Lewandowski Z. Scaling up microbial fuel cells. Environ Sci Technol 2008;42:7643–8.
[38] Di Lorenzo M, Scott K, Curtis TP, Head IM. Effect of increasing anode surface area on the performance of a single chamber microbial fuel cell. Chem Eng J 2010;156:40–8.
[39] Merkey BV, Chopp DL. The performance of a microbial fuel cell depends strongly on anode geometry: a multidimensional modeling study. Bull Math Biol 2012;74:834–57.
[40] Merkey BV, Chopp DL. Modeling the impact of interspecies competition on performance of a microbial fuel cell. Bull Math Biol 2014;76:1429–53.
[41] Luyben WL. Process modeling, simulation, and control for chemical engineers. International Edition. 2nd ed. Singapore: McGraw-Hill Publisbing Co; 1996. xxi + 741.
[42] Rice RG, Do DD. Applied mathematics and modeling for chemical engineers. New York, USA: John Wiley & Sons, Inc; 1995.
[43] Henze M, Gujer W, Mino T, van Loosdrecht M. Activated sludge models ASM1, ASM2, ASM2d and ASM3. IWA task group on mathematical modelling for design and operation of biological wastewater treatment. London: IWA; 2000.
[44] Wainwright J, Mulligan M. Environmental modeling: finding simplicity in complexity. xxii + 432. Chichester, England: John Wiley & Sons Ltd; 2004.
[45] Khine MS, Saleh IM. Models and modeling in science education. Heidelberg, Germany: Springer; 2011. ix + 300.
[46] Jorgensen SE, Bendoricchio G. Fundamentals of ecological modeling. 3rd ed. Oxford, UK: Elsevier Science Ltd.; 2001. xii + 543.
[47] Wolkenhauer O, Shibata D, Mesarovic MD. The role of theorem proving in systems biology. J Theor Biol 2012;300:57–61.
[48] Wolkenhauer O. The role of theory and modeling in medical research. Front Physiology 2013;4:377.
[49] Wolkenhauer O. Why model? Front Physiology 5, vol. 21; 2014. p. 1–5.
[50] Castellan GW. Physical chemistry. 2nd ed. Addison-Wesley; 1971.
[51] Schroder U. Anodic electron transfer mechanisms in microbial fuel cells and their energy efficiency. Phys Chem Chem Phys 2007;9:2619–29.
[52] Bronshtein I, Semendaiev K. Manual de matemáticas para ingenieros y estudiantes [Handbook of mathematics for engineers and students]. Mexico DF, Mexico: Ediciones de Cultura Popular S.A.; 1977. Spanish translation of the book published in English by MIR editorial, USSR, 1973.

[53] Perry R. Chemical engineers Handbook. 5.50 & ff. 4th ed. New York: McGraw-Hill Co; 1963.
[54] Hernandez-Flores G, Poggi-Varaldo HM, Solorza-Feria O, Romero-Castañón T, Ríos-Leal E, Galíndez-Mayer J, et al. Batch operation of a microbial fuel cell equipped with alternative proton exchange membrane. Article submitted to International Journal of Hydrogen Energy 2015. http://dx.doi.org/10.1016/j.ijhydene.2015.06.057.
[55] Poggi-Varaldo HM, Valdés L, Esparza-García FJ, Fernández-Villagómez G. Solid substrate anaerobic co-digestion of paper mill sludge, bio-solids, and municipal solid waste. Water Sci Technol 1997;35:197–204.
[56] Poggi-Varaldo HM, Rinderknecht-Seijas N. A differential availability enhancement factor for the evaluation of pollutant availability in soil treatments. Acta Biotechnol 2003;23:271–80.
[57] APHA. Standard methods for examination of water and wastewater. 17th ed. Washington DC: APHA-AWWA-WEF; 1989.
[58] Galíndez-Mayer J, Ramón-Gallegos J, Ruiz-Ordaz N, Juárez-Ramírez C, Salmerón-Alcocer A, Poggi-Varaldo HM. Phenol and 4-chlorophenol biodegradation by yeast *Candida tropicalis* in a fluidized bed reactor. Biochem Eng J 2008;38:147–57.
[59] Poggi-Varaldo HM, Alzate-Gaviria LM, Perez-Hernandez A, Nevarez-Morillon VG, Rinderknecht-Seijas N. A side-by-side comparison of two systems of sequencing coupled reactors for anaerobic digestion of the organic fraction of municipal solid waste. Waste Manage Res 2005;23(3):270–80.
[60] Valdez-Vazquez I, Poggi-Varaldo HM. Alkalinity and high total solids affecting H_2 production from organic solid waste by anaerobic consortia. Int J Hydrogen Energy 2009;34:3639–46.
[61] Kano T, Suito E, Hishida K, Miki N. Effect of microscale surface geometry of electrodes on performance of microbial fuel cells. Jpn J Appl Phys 2012;51(6):1349–51.
[62] Garibay-Orijel C, Ríos-Leal E, García-Mena J, Poggi-Varaldo HM. 2,4,6 trichlorophenol and phenol removal in methanogenic and partially-aerated methanogenic conditions in a fluidized bed bioreactor. J Chem Technol Biotechnol 2005;80:1180–7.
[63] Garibay-Orijel C, Hoyo-Vadillo C, Ponce-Noyola T, García-Mena J, Poggi-Varaldo HM. Impact of long-term partial aeration on the removal of 2,4,6-trichlorophenol in an initially methanogenic fluidized bed bioreactor. Biotechnol Bioeng 2006;94(5):949–60.
[64] Montgomery D. Design and analysis of experiments. 3rd ed. New York: John Wiley & Sons; 1991.
[65] Poggi-Varaldo HM, Munoz-Paez KM, Escamilla-Alvarado C, Robledo-Narváez PN, Ponce-Noyola MT, Calva-Calva G, et al. Biohydrogen, biomethane and bioelectricity as crucial components of biorefinery of organic wastes: a review. Waste Manag Res 2014;32:353–65. http://dx.doi.org/10.1177/0734242X14529178.

Nomenclature

A'_s: relationship between the anode surface area to cell volume, also known as specific surface area of the anode
A_{anode}: surface area of the anode
A_{cat}: area of the cathode
A_{el}: electrode surface area
A_p: actual surface area of the particle
b: moles of electrons harvested from the COD or substrate
C: conductance
CE: coulombic efficiency
COD: chemical oxygen demand
DC: direct current
$\overline{D_P}$: Average particle diameter, defined as the diameter of a sphere of the same volume as the particle
E_{anode}: anodic potential
emf: electromotive force
E_{MFC}: voltage delivered by the cell
$E_{MFC,max}$: cell potential at which the maximum volumetric power is registered
$E_{MFC,OC}$: cell potential value at open circuit potential
F: Faraday constant
GF: graphite flakes
GR: graphite rod
GT: triangles of graphite
i: current density
I: current intensity of the MFC
I_{cat}: current density per surface area of cathode
L: thickness of the anode in Di Lorenzo et al. [38].
LD: level of detection
I_{MFC}: current intensity of the MFC
M: total mass of anodic material loaded into the *MFC*
M_S: molar weight of substrate
m_{ave}: average value of the particle mass
MFC: microbial fuel cell
m_p: average weight of a particle of the given size fraction
N: total number of particles
NA: not applicable
OCP: open circuit potential
P_{An}: surface power densities
P_{cath}: power density based on surface area of electrode (cathode)
P_V: volumetric power
$P_{v,max}$: maximum volumetric power
R_{ext}: external resistance
R_{int}: internal resistance
RVC: reticulated vitreous carbon
S: specific surface or area of particle surface per unit volume of bed $= S_0 (1-\varepsilon)$
s: slope of the polarization curve defined in Di Lorenzo et al. [38].
S_0: area of particle surface per unit volume of solids
SHE: standard hydrogen electrode
SR-In: sulphate-reducing inocula
V: geometric volume or net volume
V_p: volume of the particle
V_{cell}: geometric volume of the cell chamber
wt: weight

Greek characters

β: decimal quantity in Eq. (31)
ε: void space: fractional free volume
κ: conductivity of the influent in Di Lorenzo et al. [38].
$\varnothing_s$: shape factor of the particle (also called sphericity factor)
σ: electrolytic conductivity
ρ: actual density of the solid material
ρ_{app}: apparent density
η: efficiency defined in Di Lorenzo et al. [38].
ν: variable defined by Di Lorenzo et al. [38] shown in Eq. (46) of this article